Paper 44-1 has been designated as a Distinguished Paper at Display Week 2018. The full-length version of this paper appears in a Special Section of the *Journal of the Society for Information Display (JSID)* devoted to Display Week 2018 Distinguished Papers. This Special Section will be freely accessible until December 31, 2018 via:

http://onlinelibrary.wiley.com/page/journal/19383657/homepage/display_week_2018.htm

Authors that wish to refer to this work are advised to cite the full-length version by referring to its DOI:

https://doi.org/10.1002/jsid.662

Motion-blur-free LCD for High Resolution Virtual Reality Displays

Fangwang Gou,[1] Haiwei Chen,[1] Ming-Chun Li,[2] Seok-Lyul Lee,[2] and Shin-Tson Wu,[1]

[1]College of Optics and Photonics, University of Central Florida, Orlando, Florida 32816, USA

[2]AU Optronics Corp., Hsinchu Science Park, Hsinchu 30078, Taiwan

Abstract

A new liquid crystal display device with fast response time, high transmittance, and low voltage for virtual reality is reported. When driven at 90Hz with 17% duty ratio, the motion picture response time is 1.5 ms, similar to CRT, leading to indistinguishable motion blur. Moreover, this device enables high resolution density because only one thin-film transistor per pixel is needed and it has a built-in storage capacitor.

Keywords

Vertical alignment; Fringe field switching (FFS); Liquid crystal displays (LCDs); Virtual reality.

1. Introduction

The recent rapid growth of virtual reality (VR) head mounted displays has triggered an urgent need for display devices with high resolution density and fast response time [1, 2]. In a VR system, a lens is used to magnify the displayed images. Thus, if the display resolution density is inadequate, the observer will see the screen door effect. In order to achieve field of view > 70° and to minimize the screen door effect, VR displays require resolution density over 2000 pixels per inch (PPI). At this stage, such a high PPI can be achieved by silicon-based OLED microdisplays [3] and by some LCD panels fabricated with glass-based process and special pixel design [4]. In general, OLED is a current driven device, and it requires 3-4 TFTs and 2 capacitors per pixel. On the other hand, LCD is voltage-driven and it only requires one switching TFT and one storage capacitor per pixel. Thus, LCD has potential to achieve higher resolution density than OLED for VR applications. However, traditional LCD modes, such as in-plane switching (IPS) and fringe field switching (FFS) suffer from slow response time, which results in motion blurs.

To speed up the response times, several approaches have been proposed, including polymer-stabilized blue phase LCs [5] and uniform lying helix (ULH) LCs based on flexoelectro-optic effect [6]. Each technology has its own pros and cons. For example, blue phase LC offers submillisecond response time, but it requires protruded electrodes to achieve 75% transmittance at 15 V. On the other hand, ULH LC needs complicated molecular alignment process and its highest achievable contrast ratio so far is only ~500:1. For nematic devices, low viscosity LC together with an ultra-thin cell gap (d = 1.2 μm) could achieve submillisecond response time in a reflective liquid-crystal-on-silicon device [7]. On the device side, triode approach [8-10] enables fast rise time and decay time, but it requires two TFTs per pixel and the transmittance is compromised.

In this paper, we report a VA⊕FFS mode which is driven by the longitudinal field and the fringing field. The top substrate has a common electrode, while the bottom substrate consists of FFS structure, but with etched rounded-square hole patterns on the pixel electrode. The motion picture response time is 1.5 ms at 90 Hz with 17% duty ratio, leading to indistinguishable motion picture blur. Besides, our device enables a high aperture ratio because only one TFT is needed per pixel while the bottom FFS electrodes have built-in storage capacitors. As a result, high resolution is achievable. This device is attractive for the emerging VR display applications.

2. Results and Discussion

2.1 Device Structure

Figure 1 illustrates the proposed structure. The top substrate has a planar common electrode (50 nm thick) grounded at V = 0. The bottom substrate (Fig. 1(a)) consists of three layers: 50-nm transparent planar common electrode (V = 0), a 400-nm passivation layer, and 50-nm pixel electrode with rounded-square holes. The LC material we used for simulation is ZOC-7003 (JNC, Japan) [11], which has a negative dielectric constant ($\Delta\varepsilon = -4$). Figure 1(b) shows the patterns and dimensions of the holes. The electrode gap (g) is 3μm and electrode width (w) is 4μm. The bottom electrode configuration is similar to the fringing field switching (FFS) [12], except for the patterned rounded-square holes and the LC with $\Delta\varepsilon<0$ is in vertical alignment (VA).

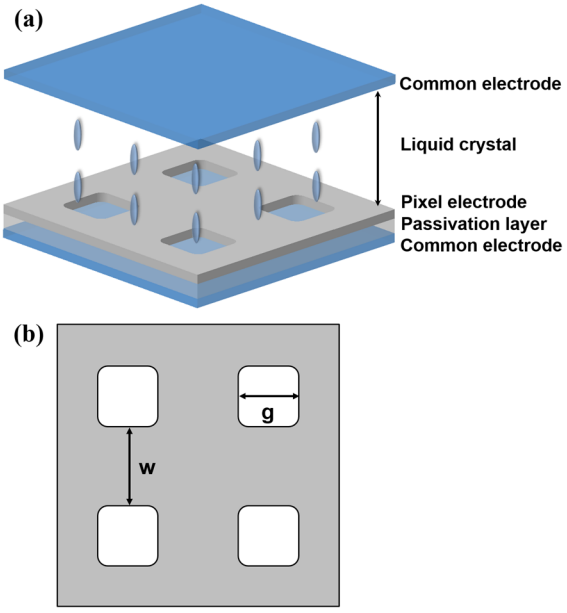

Fig. 1. (a) Device structure of the proposed VA⊕FFS cell, and (b) top view of the pixel electrode.

2.2 Voltage-dependent Transmittance

To achieve high transmittance and good dark state for wide-view purpose, the LC cell is sandwiched between two circular polarizers and a set of compensation films. When the voltage is not present, all the LC directors are vertically aligned (pre-tilt angle = 0°), as Fig. 1(a) depicts. The light passing through the LC layer experiences no phase retardation and is blocked by the crossed circular polarizers, leading to an excellent dark state. As the voltage exceeds a threshold, the LC directors are reoriented by the vertical field outside the hole area and the fringing field surrounding the hole area. For convenience, let us call this hybrid operation mode as VA⊕FFS. Similar to patterned vertical alignment (PVA) mode [13], the oblique component of the fringing field prevents LC directors from reorienting randomly even though the pre-tile angle is 0°. Figures 2(a) and 2(b) depict

the top view and cross-sectional view of LC director distributions, respectively, at a voltage-on state (7 V_{rms}). Because of symmetry, the LC directors at the center of the square holes and the pixel electrodes do not reorient (if the voltage is not too high), which function as standing walls to provide strong restoring force for improving decay time [14]. On the downside, these vertical standing walls decrease the transmittance, thus, their dimensions should be optimized. Also through simulation, we found that the pixel electrode with rounded-square holes exhibits similar performance with circular and square holes [15], indicating that our VA⊕FFS mode enables a relatively large fabrication tolerance.

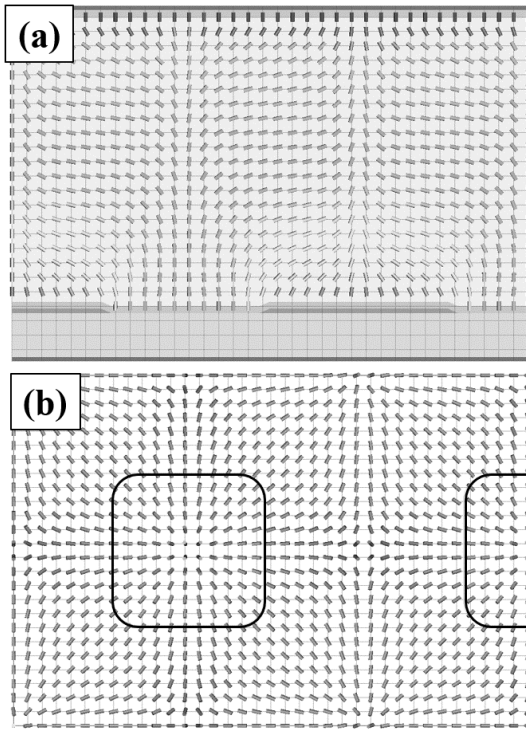

Fig. 2. Top view and (b) cross-sectional view of simulated LC director distributions of the VA⊕FFS cell at 7V_{rms}.

From Fig. 2, we can see that the LC directors inside the hole area are primarily affected by the symmetric fringing fields so that they are radially distributed. However, on top of pixel electrodes, the LC directors are influenced by both longitudinal and fringing fields. Because of these spatially nonuniform LC reorientations, crossed circular polarizers are preferred to achieve high transmittance. Figure 3 illustrates the top view of transmittance profiles with crossed linear polarizers and circular polarizers. For linear polarizers, the light transmitting though the first polarizer experiences no phase retardation if the LC directors distributed along the transmission axis of linear polarizer. As a result, the light will be blocked by the analyzer, leading to transmittance dead zone shown in Fig. 3(a). In the case of crossed circular polarizers (Fig. 3(b)), the circularly polarized light is independent of the LC director's orientation angle, thus a higher transmittance is achieved.

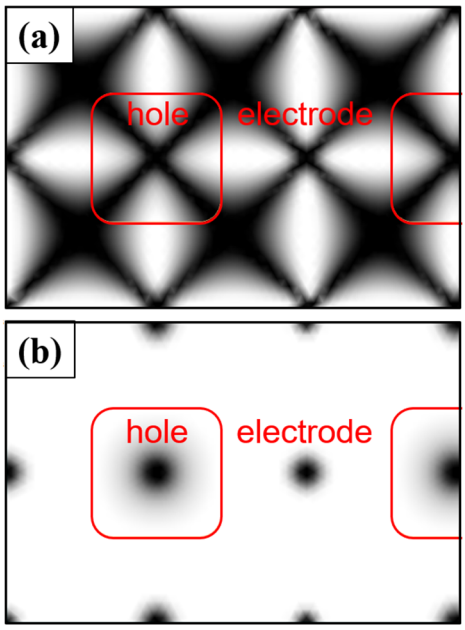

Fig. 3. Top view of on-state transmittance profiles of the VA⊕FFS cell with crossed (a) linear polarizers and (b) circular polarizers, at V_{on} = 7 V_{rms}.

Figure 4 depicts the simulated VT curves of our optimized VA⊕FFS cell at λ = 450nm, 550nm and 650nm. By using circular polarizers, the peak transmittance can reach 85% at 7Vrms for λ = 550 nm, which is comparable to the 2-domain nFFS mode (~85%).

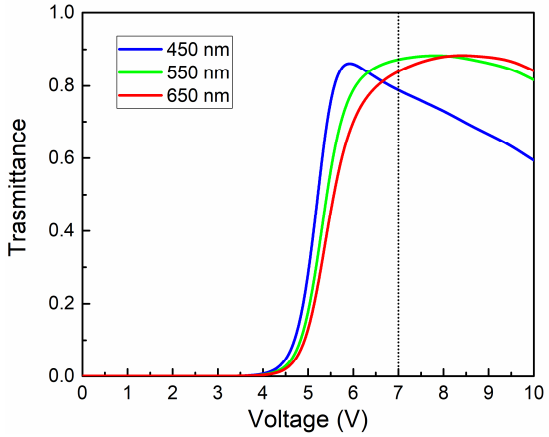

Fig. 4. Simulated VT curves of the proposed VA⊕FFS cell at the specified wavelengths. *d* = 3.5 μm, *w* = 4 μm, and *g* = 3 μm.

2.3 Response Time

To obtain the gray-to-gray (GTG) response time of our VA⊕FFS cell, we divided the VT curve at λ = 550 nm into 256 gray levels and calculated the response time between different gray levels. The response time is defined as the time interval between 10% and 90% transmittance change. Results are shown in Figure 5. By applying overdrive and undershoot driving scheme [16], the average GTG response time is 2.26 ms and the slowest LC response time 4.07 ms.

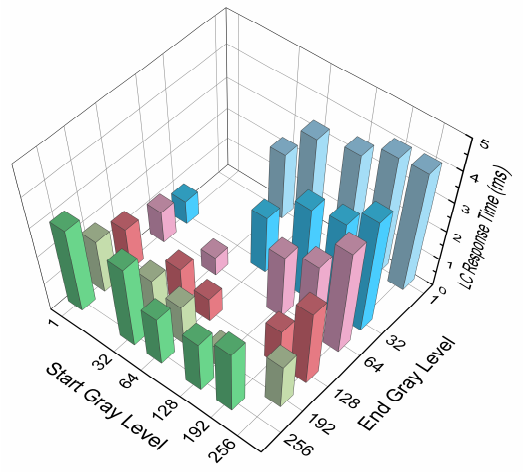

Fig. 5. The GTG response time of the VA⊕FFS mode.

In a sample-and-hold type TFT LCD, motion image blur is determined jointly by the LC response time as well as TFT frame rate (f). To quantify the visual performance of a moving object on the screen, motion picture response time (MPRT) has been proposed [17]. Recently, a simple yet accurate analytical equation relating MPRT with LC response time and frame rate has been derived [18]:

$$MPRT \approx \sqrt{\tau^2 + (0.8T_f)^2}. \quad (1)$$

Here, τ is the LC response time and T_f (= 1000/f) is the TFT frame time. The average MPRT for the VA⊕FFS LCD at f = 90 Hz is 9.22 ms.

To mitigate image blur, MPRT should be <1.5 ms, like CRT (cathode ray tube). But from Eq. (1), we know that even if LC response time is zero (τ = 0 ms), the MPRT is still as slow as 8.89 ms at f = 90 Hz. This happens to OLED as well. One way to reduce MPRT is to increase frame rate. Figure 6 shows MPRT versus LC response time at different frame rates. As frame rate increases, MPRT decreases almost linearly. When f = 480 Hz, the average MPRT is 2.88 ms, which is still too slow. Moreover, for a high resolution LCD, e.g. 4K2K, operating at 480 Hz frame rate would demand a very short TFT charging time (1.08 μs). This is technically challenging by itself.

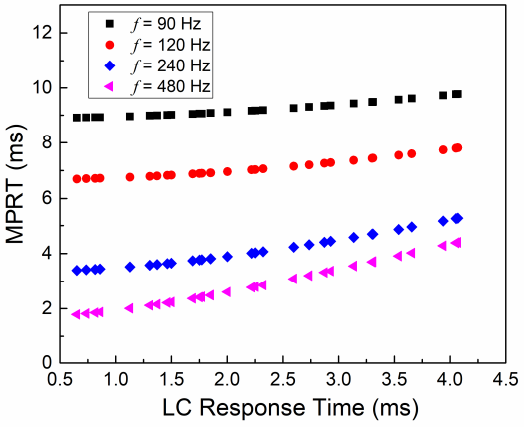

Fig. 6. MPRT as a function of LC response time at different frame rates.

A simpler method to reduce MPRT is through backlight modulation [19]. In one frame time, the backlight remains off during gate line scanning and LC transition time, and then is turned-on when all of the pixels have fully reached their targeted gray levels. As a result, the initial slow transition part of LC is obscured by the delayed backlight, which effectively suppresses the sample-and-hold effect. Such an operation mechanism is similar to impulse driving of CRT. The on-time ratio of the backlight is defined as duty ratio (DR), and it satisfies:

$$T_f \times DR = T_f - T_g - T_{LC}, \quad (2)$$

where T_g is the gate scan time and T_{LC} is the slowest LC reponse time. Therefore, MPRT can be simplified as:

$$MPRT \approx 0.8 \times (T_f - T_g - T_{LC}). \quad (3)$$

For example, if our device is driven at f = 90 Hz (T_f = 11.11 ms) and T_g takes 5 ms, in order to obtian MPRT ≈ 1.5 ms, the required time for turning on the backlight should be less than 4.24 ms, indicating DR = 17%. From Eq (3), we can obtain the remaing time for LC response time is 4.23, which is larger than the slowest LC repsonse time of our VA⊕FFS mode (4.07 ms). Therefore, our VA⊕FFS mode can achieve indistinguishable motion blur. If we further increase frame rate to 120 Hz with the same duty ratio, the MPRT will decrease to 1.13 ms, and the slowest LC response time should be less than 1.92 ms. To do so, we could employ a LC material with higher Δn and lower viscosity. However, the latter may lead to a smaller Δε, which in turn results in slightly higher on-state voltage.

2.3 Viewing Angle

To widen the viewing angle of an LCD, compensation films together with a directional backlight and a weak diffusive film are employed [20]. Normally, for multi-domain vertical-alignment (MVA) LCDs, a biaxial film or a pair of positive A and positive C uniaxial films are often used. While for VA⊕FFS mode, we used circular polarizers instead of linear polarizers in order to obtain high transmittance. Therefore, compensation design for circular polarizers is required. In our simulation, we used the compensation scheme proposed by Ge, et al. [21]. First, a negative C-plate is used to partially compensate the phase retardation from the LC layer. After optimization, a biaxial plate is added to compensate the residual phase retardation from the negative C-plate and the LC layer. The parameters of the negative C-plate and biaxial plate are as follows: $n_{e,C}$ = 1.5902, $n_{o,C}$ = 1.5866, $n_{x,B}$ = 1.5028, $n_{y,B}$ = 1.5000, $n_{z,B}$ = 1.5018, d_C = 21.4 μm, d_B = 74.0 μm. For the directional backlight, it has a narrow angular luminance distribution: + 10°/-10° in the x direction (φ = 0~180°) and + 11°/-10° in the y direction (φ = 90~270°). Figure 7 depicts the calculated isocontrast contour of our VA⊕FFS LCD. The maximum contrast ratio is ~4800:1 and a contrast ratio over 1000:1 is expanded to ~60° viewing cone.

In addition to wide view, gamma shift is another important concern for display devices. To quantitatively evaluate the off-axis image quality, an off-axis image distortion index (D) defined in [22] is used. When D < 0.2, the image distortion is indistinguishable by the human eye. With the directional backlight and diffusive film, we could achieve D = 0.147. Besides, the diffusive film could be replaced by a quantum dot array to widen the viewing angle while keeping a wide color gamut [23].

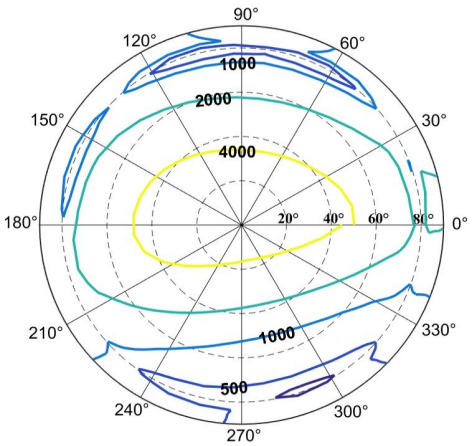

Fig. 7. Simulated isocontrast contour at viewing angle θ = 0°, 20°, 40°, 60° and φ = 0° with a directional backlight and compensation films.

3. Conclusion

Our proposed VA⊕FFS mode exhibits several attractive properties: peak transmittance >85% and low operation voltage (7V) by using circular polarizers, and potentially high resolution density (single TFT per pixel). By increasing the driving frequency to 90 Hz and decreasing the duty ratio to 17%, we obtained MPRT ≈1.5 ms, which is comparable to CRT. Potential application of our VA⊕FFS for the wearable VR displays is foreseeable.

4. Acknowledgements

The authors are indebted to a.u.Vista, Inc. for the financial support.

5. References

[1] O. Cakmakci and J. Rolland, "Head-worn displays: a review," J. Disp. Technol., 2, No. 3,199-216 (2006).

[2] S. Kawashima et al., "A 1058-ppi 4K ultrahigh-resolution and high aperture LCD with transparent pixels using OS/OC technology," SID Int. Symp. Digest Tech. Papers., 48, No. 1, 242-245 (2017).

[3] A. Ghosh et al., "Directly patterned 2645 PPI full color OLED microdisplya for head mounted wearables," SID Int. Symp. Digest Tech. Papers., 47, No. 1, 837-840 (2016).

[4] H. S. Lee, et al., "An Ultra High Density 1.96" UHD 2250ppi Display," SID Int. Symp. Digest Tech. Papers., 48, No. 1, 403-405 (2017).

[5] H. Kikuchi, M. Yokota, Y. Hisakado, H. Yang, and T. Kajiyama, "Polymer-stabilized liquid crystal blue phases," Nat. Mater. **1**, 64–68 (2002).

[6] J. S. Patel and R. B. Meyer, "Flexoelectric electro-optics of a cholesteric liquid crystal," Phys. Rev. Lett. **58**, 1538–1540 (1987).

[7] H. Chen, F. Gou, and S. T. Wu, "A submillisecond-response nematic liquid crystal for augmented reality displays," Opt. Mater. Express **7**, 195–201 (2017).

[8] D. J. Channin, "Triode optical gate: A new liquid crystal electro-optic device," Appl. Phys. Lett. **26**, 603– 605 (1975).

[9] Y. Iwata, M. Murata, K. Tanaka, A. Jinda, T. Ohtake, T. Shinomiya, and H. Yoshida, "Novel super-fast- response, ultra-wide temperature range VA-LCD," SID Int. Symp. Digest Tech. Papers **44**, 431–434 (2013).

[10] T. H. Choi, Y. J. Park, J. W. Kim, and T. H. Yoon, "Fast grey-to-grey switching of a homogeneously aligned liquid crystal device," Liq. Cryst. **42**, 492–496 (2015).

[11] Y. Chen, F. Peng, T. Yamaguchi, X. Song, and S. T. Wu, "High performance negative dielectric anisotropy liquid crystals for display applications," Crystals **3**, 483–503 (2013).

[12] S. H. Lee, S. L. Lee, and H. Y. Kim, "Electro-optic characteristics and switching principle of a nematic liquid crystal cell controlled by fringe-field switching," Appl. Phys. Lett. **73**, 2881–2883 (1998).

[13] K. H. Kim, K. H. Lee, S. B. Park, J. K. Song, S. N. Kim, and J. H. Souk, "Domain divided vertical alignment mode with optimized fringe field effect," Proc. Asia Display **98**, 383–386 (1998).

[14] H. Chen, G. Tan, Y. Huang, Y. Weng, T. H. Choi, T. H. Yoon, and S. T. Wu, "A low voltage liquid crystal phase grating with switchable diffraction angles," Sci. Rep. **7**, 39923 (2017).

[15] F. Gou, H. Chen, M. C. Li, S. L. Lee, and S. T. Wu, "Submillisecond-response liquid crystal for high-resolution virtual reality displays," Opt. Express **25**, 7984-7997 (2017)

[16] S. T. Wu, "Nematic liquid crystal modulator with response time less than 100 μs at room temperature," Appl. Phys. Lett. **57**, 986–988 (1990).

[17] Y. Igarashi, T. Yamamoto, Y. Tanaka, J. Someya, Y. Nakakura, M. Yamakawa, S. Hasegawa, Y. Nishida, and T. Kurita, "Summary of moving picture response time (MPRT) and futures," SID Int. Symp. Digest Tech. Papers **35**, 1262–1265 (2004).

[18] F. Peng, H. Chen, F. Gou, Y. H. Lee, M. Wand, M. C. Li, S. L. Lee, and S. T. Wu, "Analytical equation for the motion picture response time of display devices," J. Appl. Phys. **121**, 023108 (2017).

[19] H. Ito, M. Ogawa, and S. Sunaga, "Evaluation of an organic light-emitting diode display for precise visual stimulation," J. Vis. **13**, 6 (2013).

[20] K. Käläntär, "A directional backlight with narrow angular luminance distribution for widening the viewing angle for an LCD with a front-surface light-scattering film," J. Soc. Inf. Disp. **20**, 133–142 (2012).

[21] Z. Ge, R. Lu, T. X. Wu, S. T. Wu, C. L. Lin, N. C. Hsu, W. Y. Li, and C. K. Wei, "Extraordinarily wide-view circular polarizers for liquid crystal displays," Opt. Express **16**, 3120–3129 (2008).

[22] S. S. Kim, B. H. Berkeley, K. H. Kim, and J. K. Song, "New technologies for advanced LCD-TV performance," J. Soc. Inf. Disp. **12**, 353–359 (2004).

[23] J. P. Yang, E. L. Hsiang, and H. M. Philip Chen, "Wide viewing angle TN LCD enhanced by printed quantum- dots film," SID Int. Symp. Digest Tech. Papers **47**, 21–24 (2016).